The neural dynamics of positive and negative expectations of pain

Authors: Christoph A. Wittkamp[1], Maren-Isabel Wolf[1], Michael Rose*

Department of Systems Neuroscience, University Medical Center Hamburg-Eppendorf

[1] These authors contributed equally to this work.

*** Correspondence address:**

Department of Systems Neuroscience, University Medical Center Hamburg-Eppendorf

Martinistr. 52, Building W34

20248 Hamburg, Germany

Phone: +49-40-7410-54730, Fax: +49-40-7410-59955

Email: rose@uke.de

Abstract

Pain is heavily modulated by expectations. Whereas the integration of expectations with sensory information has been examined in some detail, little is known about how positive and negative expectations are generated and their neural dynamics from generation over anticipation to the integration with sensory information. The present preregistered study employed a novel paradigm to induce positive and negative expectations on a trial-by-trial basis and examined the neural mechanisms using combined EEG-fMRI measurements (n=50). We observed substantially different neural representations between the anticipatory and the actual pain period. In the anticipation phase i.e., before the nociceptive input, the insular cortex, dorsolateral prefrontal cortex (DLPFC), and anterior cingulate cortex (ACC) showed increased activity for expectations regardless of their valence. Interestingly, a differentiation between positive and negative expectations within the majority of areas only occurred after the arrival of nociceptive information. FMRI-informed EEG analyses could reliably track the temporal sequence of processing showing an early effect in the DLPFC, followed by the anterior insula and late effects in the ACC. The observed effects indicate the involvement of different expectation-related subprocesses, including the transformation of visual information into a value signal that is maintained and differentiated according to its valence only during stimulus processing.

1. Introduction

Nociceptive input can result in highly variable sensations of pain with expectations playing a crucial role in pain modulation (Atlas & Wager, 2012). Positive expectations can lead to hypoalgesia (placebo effect), while negative expectations can increase the perceived intensity of pain (nocebo effect; Kong & Benedetti, 2014). Although many studies have shown that expectations can influence pain perception, the neuronal processes underlying the generation of expectations prior to the appearance of the pain stimulus are not yet fully understood (Benedetti, 2014; Büchel et al., 2014; Koyama et al., 2005; Wager & Atlas, 2015). Several studies have demonstrated that placebo and nocebo effects influence brain activity during pain perception (Egorova et al., 2015; Wager & Atlas, 2015; Zunhammer et al., 2021). This may occur through multiple pathways that are involved in integrating expectations and sensory information (Geuter et al., 2017). Especially the descending pain modulatory system (DPMS; Geuter et al., 2017; Tu et al., 2022) is associated with placebo and nocebo effects and is thought to consist of areas like the periaqueductal grey (PAG), dorsolateral prefrontal cortex (DLPFC), anterior cingulate cortex (ACC), and amygdala (Eippert et al., 2009), as well as frontal areas like the vmPFC (Geuter et al., 2017; Tu et al., 2022). Further, placebo and nocebo effects modulate activity in areas classically associated with pain processing like the thalamus and the insula during noxious stimulation (Atlas & Wager, 2014; Wager & Atlas, 2015; Wager et al., 2004; Zunhammer et al., 2021).

A central feature of expectations is that they are generated prior to the appearance of the stimulus and should therefore be reflected in anticipatory neural activity (Kong et al., 2007; Wager et al., 2004). The mere expectation of the appearance of a painful stimulus has been shown to activate regions relevant to

subsequent pain processing, such as the insula, DLPFC, and thalamus (Palermo et al., 2015; Ploghaus et al., 1999). Similarly, there is evidence that expecting reduced pain (e.g. via a placebo) modulates activity in parts of the DPMS and the insula already during pain anticipation (Wager et al., 2011). This includes the DLPFC (Amanzio et al., 2013; Geuter et al., 2013; Wager et al., 2004; Watson et al., 2009) and the ACC (Amanzio et al., 2013; Geuter et al., 2013) and takes place prior to the widespread modulation of neural activity in the DPMS during pain processing (Amanzio et al., 2013; Atlas & Wager, 2014). However, it remains unclear whether this anticipatory modulation reflects only a pre-activation of later relevant networks or indicates functionally distinct processes in expectation generation. Comparing neural processing during both the anticipatory and pain periods prior to the stimulus is crucial for better dissociating the formation and maintenance of pain-related expectations from their integration with nociceptive input. (Wager et al., 2004).

Another important factor when examining the representation of expectations is their valence, i.e. whether they are positive (as in placebo effects) or negative (as in nocebo effects). It remains elusive whether positive and negative expectations share a common neural basis or depend on different networks (Freeman et al., 2015). On the basis of behavioral differences between positive and negative expectations, such as their varying correlations with the amount of prior experience and differences in learning (Colloca et al., 2010; Colloca et al., 2008), it seems reasonable to assume at least partially dissimilar neural representations of positive and negative expectations. Especially during pain perception, there is evidence of distinct neural processes for positive and negative expectations, as well as valence-dependent modulation of similar systems. More specifically, some findings suggest differential modulation of activity in key areas of the DPMS and reward system by the valence of expectations (Benedetti et al., 2020; Crawford et al., 2021; Koyama et al., 2005; Scott et al., 2008).

Alternatively, some studies have reported the absence of shared brain activations during the perception of pain (Bingel et al., 2011; Freeman et al., 2015; Fu et al., 2021; Shi et al., 2021; Shih et al., 2019). Similar findings have been reported during pain anticipation, as some areas have been reported to be specifically activated for either placebo or nocebo (Fu et al., 2021; Rossettini et al., 2023) or show opposing valence-dependent responses (Amanzio et al., 2013; Kong et al., 2008; Palermo et al., 2015). However, there is conflicting evidence of shared anticipatory activation for both placebo and nocebo in some areas of the DPMS like the DLPFC and ACC (Amanzio et al., 2013; Amanzio & Palermo, 2019; Colloca & Benedetti, 2007; Frisaldi et al., 2015; Manaï et al., 2019; Palermo et al., 2015; Rossettini et al., 2023; Schmid et al., 2015). This illustrates an ongoing debate about whether there is a common neural basis of positive and negative expectations instead of entirely separated representations (Freeman et al., 2015; Fu et al., 2021). Taken together, the neuronal representations of positive and negative expectations may consist of shared valence-neutral processes (common effects) and different or differentially modulated valence-dependent processes (distinct effects), and this relationship may change over time from the formation of expectations until their integration with the sensory information. To adequately examine common and distinct neuronal representations, it is imperative to compare positive and negative expectations against each other, as well as to a control condition devoid of any expectations. Hence, in this study, we implemented a within-subjects design in which participants were subjected to positive, negative, or no expectations on a trial-by-trial basis, enabling an exploration of common and distinct processes.

Even during the anticipation phase, it is reasonable to presume the involvement of distinct processes unfolding in a temporal sequence. For instance, the visual cue must first be encoded and transformed into an expectation signal that can be

interpreted by a “pain system”. A potential candidate for this integration process is the insula, which is recognized for its function as a multimodal network hub (Adler-Neal et al., 2019; Dionisio et al., 2019; Lu et al., 2016). Within the DPMS, prefrontal areas have been suggested to provide predictions for downstream pain-sensitive systems, implying an early role within this system (Geuter et al., 2017; Koban et al., 2017; Wager & Atlas, 2015). Subsequently, it appears plausible that other areas of the DPMS would need to be “informed” and activated in close temporal proximity to the pain stimulus in order to exert their influence on pain perception (Amanzio et al., 2013). The assessment of the temporal profile of expectancy generation is beyond the possibility of fMRI. We therefore combined fMRI with simultaneous EEG measurements, allowing us to temporally localize neural activity by utilizing the temporal and spatial advantages of both techniques at the single trial level.

In this study, we investigated the neural basis of the common and distinct processes underlying positive and negative expectations, and the formation and integration of expectations into pain perception, using a novel paradigm that allowed the manipulation of expectations on a trial-by-trial basis, while EEG and fMRI measures were recorded. We presented cues to induce expectations (positive, negative, or no expectations) followed by an anticipatory period in which different expectations emerged. This allowed us to examine the distinct and common effects of placebo and nocebo in the anticipation and pain phase by comparing the different expectation conditions. We focused on the evaluation of the different neuronal processes that contribute to the generation of expectations in the anticipatory period and the effects during pain perception, using combined EEG and fMRI.

We expected that representations of pain-related expectations undergo dynamic changes during the anticipation phase and pain phase, reflecting different

144 processes such as expectation formation, expectation integration, and pain
145 modulation. We therefore hypothesized to see dissociable neuronal representations of
146 expectations during the anticipation phase and during the pain phase, albeit in similar
147 areas. More specifically, we expected positive and negative valences to be
148 differentially represented during the anticipation phase and the pain phase.
149

150 **2. Results**

151 In total, we investigated 50 participants (32 female) in a combined EEG-fMRI
152 paradigm. In short, participants were told that they would be given real-time visual
153 feedback on their current pain sensitivity based on their EEG activity using a Brain-
154 Computer Interface (BCI). The feedback indicated one of three different brain states:
155 either a state of high pain sensitivity (red cue/nocebo condition/negative expectation),
156 low pain sensitivity (green cue/placebo condition/positive expectation), or that no
157 prediction would be made (yellow cue/control condition/no expectation). In fact, the
158 visual cues were not related to any brain activity but were only used to produce the
159 corresponding expectations. To reinforce expectations, we also performed a learning
160 (i.e. conditioning) phase. Here, red cues were paired with higher pain intensity (VAS
161 level 70), while green cues were paired with lower pain intensity (VAS level 30). In the
162 ensuing test phase (*see Figure 1*), temperatures were kept constant (VAS level 60). In
163 each trial, participants were given a BCI-based feedback supposedly related to their
164 current brain state (cue phase) and subsequently rated their pain expectation for the
165 next stimulus (expectation rating). After a fixed anticipation phase, they were presented
166 with a brief heat pain stimulus with a constant target temperature irrespective of
167 condition (pain phase), and lastly had to rate how intense they perceived the stimulus

(pain rating). Apart from EEG and fMRI we also continuously recorded electrodermal activity.

Figure 1

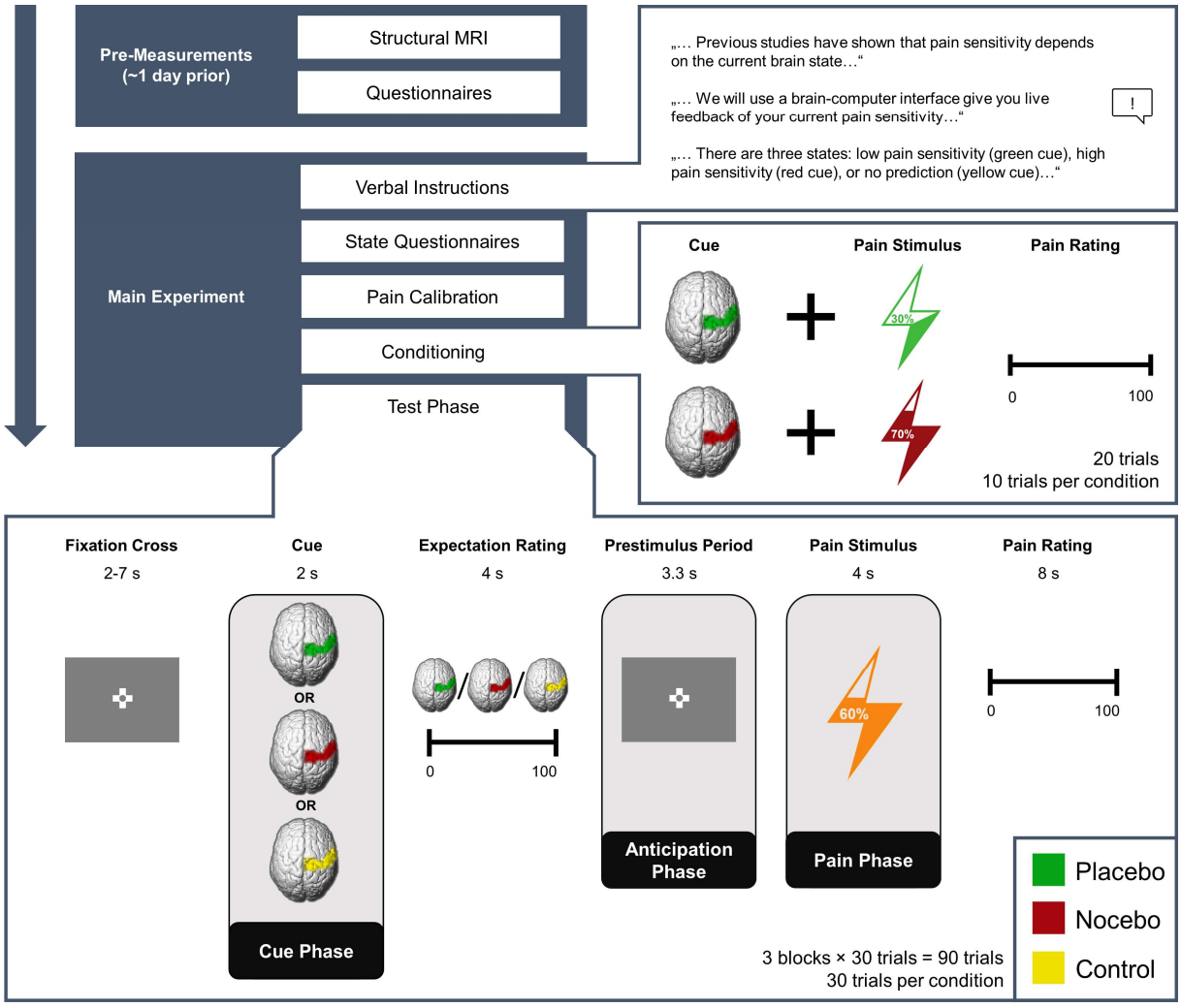

Experimental Procedure.

Structure of the experiment including pre-measurements and the main experiment. Expectations were generated using a sham BCI, i.e., participants were told that they would receive real-time feedback regarding their pain sensitivity (verbal instructions) and experienced the validity of this feedback (conditioning). In the conditioning phase, green cues were paired with lower pain intensities compared to red cues unbeknownst

179 to the participants. In the test phase, the stimulation temperature was always the same,
180 regardless of the cue. The presentation of the condition cue varied from trial to trial.
181

182 **2.1 Successful induction of placebo and nocebo effects in behavioral ratings and**
183 **skin conductance responses**

184 Our data show successfully induced expectations in line with the cued sham
185 brain states as evidenced by a significant main effect of condition in a repeated-
186 measures ANOVA for mean expectation ratings ($F_{(2,98)} = 86.51$, $p < .001$, $\eta_P^2 = .64$; *see*
187 *Figure 2A*). Expectation ratings were higher in the nocebo ($M = 65.80$, $SD = 15.80$)
188 compared to the control condition ($M = 48.58$, $SD = 13.79$, $p < .001$), which in turn
189 were higher than in the placebo condition ($M = 34.33$, $SD = 17.71$, $p < .001$). Similarly,
190 mean pain ratings were affected by our manipulation (rmANOVA: $F_{(2,98)} = 63.00$,
191 $p < .001$, $\eta_P^2 = .56$; *see Figure 2B*). Post-hoc Tukey tests revealed higher pain ratings
192 in the nocebo ($M = 56.80$, $SD = 14.21$) compared to the control condition ($M = 51.40$,
193 $SD = 14.31$, $p < .001$), which in turn led to higher pain ratings than the placebo
194 condition ($M = 44.88$, $SD = 15.06$, $p < .001$). Moreover, placebo (control - placebo) and
195 nocebo (nocebo - control) effects were significantly correlated across subjects for both
196 expectation ($r = 0.64$, $p < .001$) and pain ratings ($r = 0.30$, $p = .033$), indicating that
197 subjects who experienced stronger placebo effects also experienced larger nocebo
198 effects.

199 The expectation manipulation not only affected behavioral ratings but also the
200 skin conductance responses (SCRs) to the pain stimuli (rmANOVA: $F(2,50) = 4.33$,
201 $p = .018$, $\eta_P^2 = 0.15$; *see Figure 2C*). A posthoc Tukey test showed larger SCRs in the
202 nocebo ($M = 0.05$, $SD = 0.09$) compared to the placebo condition ($M = -0.04$,

SD = 0.10, *p* = .049). SCRs in the control condition (*M* = -0.01, *SD* = 0.07) did not significantly differ from neither nocebo (*p* = .072) nor placebo condition (*p* = .607).

Figure 2

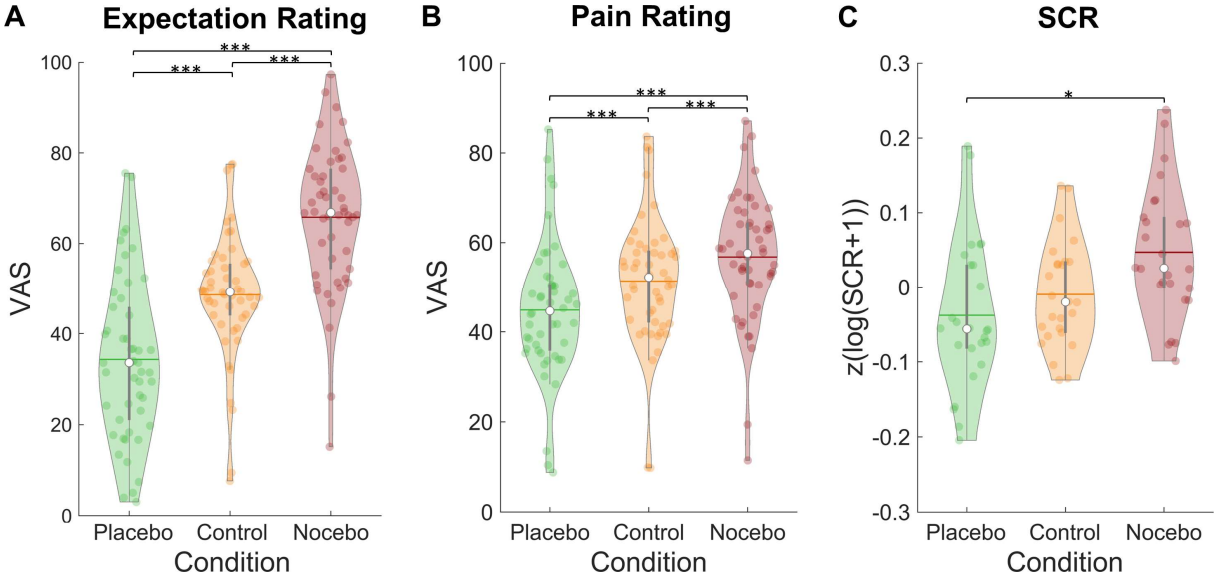

Expectation ratings, pain ratings and skin conductance response by condition. Mean expectation **(A)** and pain ratings **(B)** on a visual analogue scale separately for each condition. **(C)** Mean skin conductance responses in the three conditions. White dots = mean, horizontal lines = median, thick grey vertical lines = upper and lower quartile, coloured dots = pain ratings of individual participants per condition.
* *p* < .05. ** *p* < .01. *** *p* < .001.

2.2 Successful induction of expectation effects in fMRI pattern

Induction of expectation effects was also tested in functional imaging data. For all fMRI analyses, a finite impulse response (FIR) model was used to characterize BOLD fluctuations over time from cue onset to the pain rating (*see Methods for details*). The stimulus intensity independent pain signature (SIIPS) has been introduced as a marker for subjective pain perception going beyond intensity differences as it has been

reported to be affected by psychological factors such as expectations (Botvinik-Nezer et al., 2023; Woo et al., 2017). To further validate our experimental design, we estimated the SIIPS score for each condition during the pain phase as a marker for differences in pain perception between the three conditions (see Methods). A rmANOVA revealed significant differences between the three conditions within the pain period ($F(2,88) = 11.59$, $p < .001$, $\eta_P^2 = 0.21$), with Bonferroni-corrected paired *t*-tests showing significant differences between the placebo and nocebo condition ($t_{(44)} = 4.79$, $p < .001$) and between the nocebo condition and the control condition ($t_{(44)} = 3.36$, $p = .002$) but not between the control and the placebo condition ($t_{(44)} = 1.35$, $p = .184$, see *Figure 3*). We therefore conclude that the manipulation of expectations led to significant perceptual differences. Contrastingly, the SIIPS signature failed to discern between conditions during the anticipation period, suggesting fundamentally distinct processes in the two phases ($F(2,88) = 0.79$, $p = .455$, $\eta_P^2 = 0.02$).

Figure 3

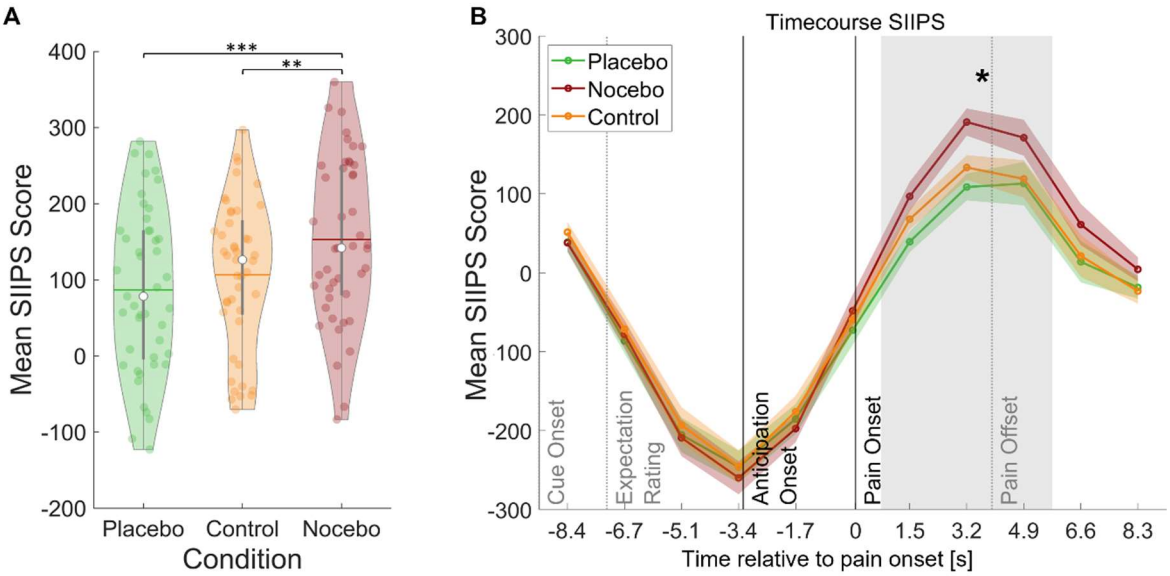

SIIPS scores by condition.

238 **(A)** Mean SIIPS score per condition for all time-points during pain perception. White
239 dots = mean, horizontal lines = median, thick grey vertical lines = upper and lower
240 quartile, coloured dots = pain ratings of individual participants per condition. * $p < .05$.
241 ** $p < .01$. *** $p < .001$. **(B)** Mean SIIPS score per condition plotted over the duration
242 of the whole trial. The mean SIIPS scores shown in A were extracted from the grey
243 marked period.
244

245 **2.3 Neuronal representation of expectations over time**

246 In our main analysis, we found a clear dissociation between the anticipation and
247 pain phases with a predominantly common representation of positive and negative
248 expectations during the anticipation phase and a later shift towards distinct effects
249 during the pain phase (*see Figure 4A*). In order to investigate how the representations
250 of expectations changed over time from the anticipation to the pain phase, we identified
251 common (i.e., positive and negative vs. control; constrained to areas with no statistical
252 difference between positive and negative) and distinct (positive vs. negative) effects of
253 expectations in each phase (*see Supplementary Tables 1-4 for all comparisons*).
254 During the anticipation phase, common effects of expectations were found in several
255 important areas of the DPMS e.g. in the bilateral DLPFC, bilateral ACC and right
256 vmPFC, indicating that expectations were represented in a rather general and
257 nonspecific way during this period. With the stimulus onset activity these areas showed
258 differential activation between positive and negative expectations. Further differential
259 activity was observed in e.g. left insula, amygdala, thalamus, and hippocampus during
260 the pain phase.

261 Crucially, the bilateral DLPFC, right vmPFC, left anterior insula, and thalamus
262 were engaged during both the anticipation and pain phases (*see Figure 4B*). In all
263 these areas, expectations shifted from a common (positive and negative > control)

towards a distinct representation (positive > negative: bilateral DLPFC, right vmPFC, and left anterior insula; negative > positive: thalamus) over time. In addition to these areas that are frequently related to expectation effects, the right angular gyrus was also engaged throughout the time course, similarly initially showing a common representation of positive and negative expectations during the anticipation phase and differentiating only during pain perception ($p < .05$ whole-brain FWE-corrected; *see Figure 5*).

The differences between the anticipation and the pain phase demonstrate that specific expectations were mediated by different processes during these phases and arise from a dynamic interplay of brain regions such as the DLPFC, vmPFC, anterior insula, and thalamus over time.

293 **Figure 4**

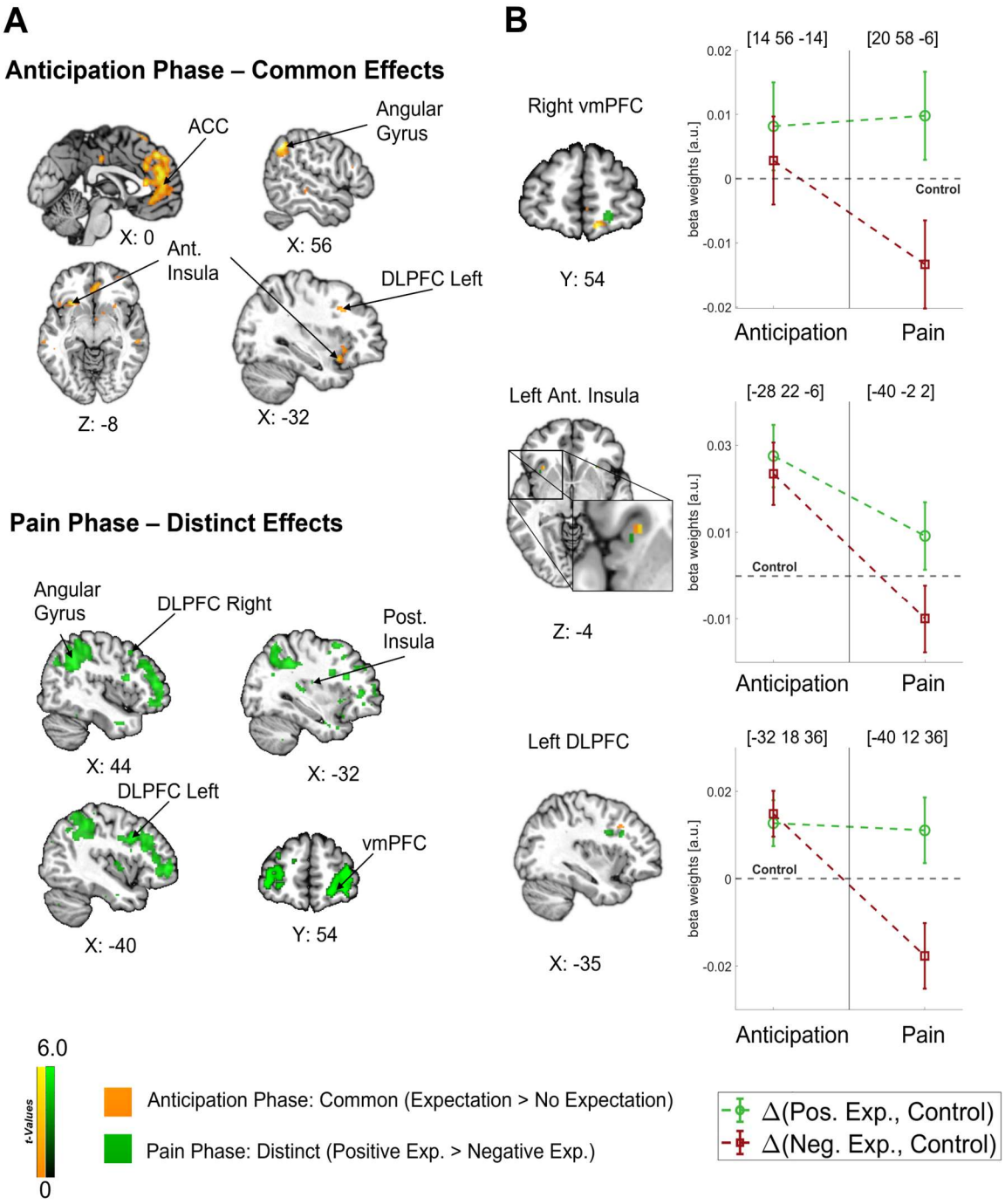

294

295 **Differentiation of effects during the anticipation and pain phase.**

296 **(A) Top:** Common effects during pain anticipation (expectation > no expectation) at
297 $p < .001$ (uncorrected for display purposes) show widespread higher activity for both
298 positive and negative expectations compared to the control condition. **Bottom:** Distinct
299 effects (positive > negative) during pain perception are shown, indicating broadly

300 higher activity for positive compared to negative expectations. **(B) Left**: For selected
301 areas, the overlap between common effects of expectations during the anticipation
302 phase (yellow) and distinct effects of positive and negative expectations during the
303 pain phase (green) in the respective area is shown. **Right**: The corresponding
304 activation levels of positive and negative expectations (i.e., beta weights from the FIR
305 model) baselined by the control condition are plotted for each phase at the respective
306 peaks (peak coordinates in parentheses). The visualization highlights the
307 differentiation of effects following the onset of pain.

308

309 **Figure 5**

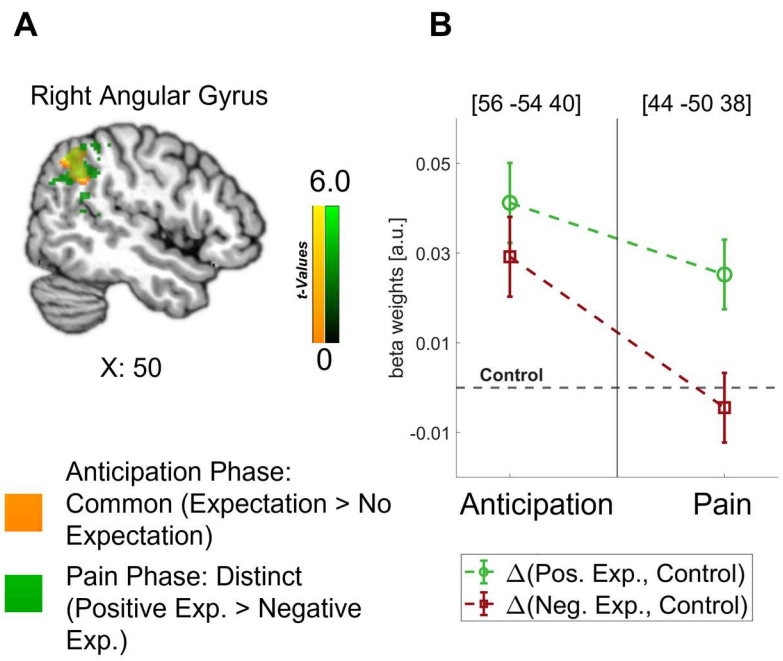

310

311 **Representation of Expectations in the Angular Gyrus.**

312 **(A)** Overlap between common effects of expectations during the anticipation phase
313 (expectation > no expectation; yellow) and distinct effects of positive and negative
314 expectations during the pain phase (positive > negative; green) is shown for the
315 angular gyrus at $p < .001$ (uncorrected for display purposes). **(B)** The corresponding

activation levels of positive and negative expectations (i.e., beta weights from the FIR model) baselined by the control condition are plotted for each phase at the respective peaks (peak coordinates in parentheses).

2.4 Timing of effects during the anticipation phase

To obtain detailed information on the temporal characteristics of the expectation effects during pain anticipation, we performed fMRI-informed EEG analyses. Specifically, we were interested in the temporal sequence of the areas involved. Single-trial estimates of fMRI activity during the anticipation phase were correlated with time-frequency decomposed EEG measures for each participant and then statistically tested at the group level. This analysis was conducted separately for the identified regions of interest that represented expectations during both the anticipation and pain phase (left anterior insula, right vmPFC, bilateral DLPFC, and thalamus). We further included the bilateral ACC, as we were interested in all areas that reflected expectations during the anticipation phase.

Clear temporal differences between areas were observed. The earliest correlation of fMRI activity with EEG oscillatory power was found in the left DLPFC already during the expectation rating at theta to low gamma frequencies in a negative direction (-6.3 until -4.4 s, 4 to 45.28 Hz; p = .007; see *Figure 6A*; additional information for all regions can be found in *Supplementary Table 5*). Next, anticipatory activity in the left anterior insula was associated with decreased EEG oscillatory power during the late expectation rating and anticipation phase (-4.4 to -2.5 s) spanning from theta to low gamma frequencies (5.67 to 32 Hz; p < .001; see *Figure 6B*). Lastly, we found a significant positive association of EEG activity with fMRI activity in the right ACC during the anticipation and early pain phase in the gamma frequency range (-3 to 0.3 s,

341 26.89 to 128 Hz; p = .003; see *Figure 6C*). As expected due to the close spatial
342 proximity, activity in the left ACC was similarly positively correlated with EEG activity
343 in the anticipation and pain phase (cluster 1: -2.3 to -1.3 s, 32 to 128 Hz; p = .019;
344 cluster 2: -0.9 to 0.3 s, 32 to 128 Hz; p = .021). We did not observe significant
345 correlations of EEG power with fMRI activity in the other ROIs.

346 In summary, the analyses indicated that areas exhibiting similar fMRI effects for
347 positive and negative expectations during the anticipation phase are linked to distinct
348 temporal and oscillatory patterns. Notably, the left DLPFC and the left anterior insula
349 displayed an early negative correlation between anticipatory activity and EEG power,
350 primarily in the lower frequency range. Conversely, the subsequent effects in the
351 bilateral ACC were associated with an increase in gamma oscillations and were
352 observed at later time points during the anticipation phase indicating different
353 processes.

354

Figure 6

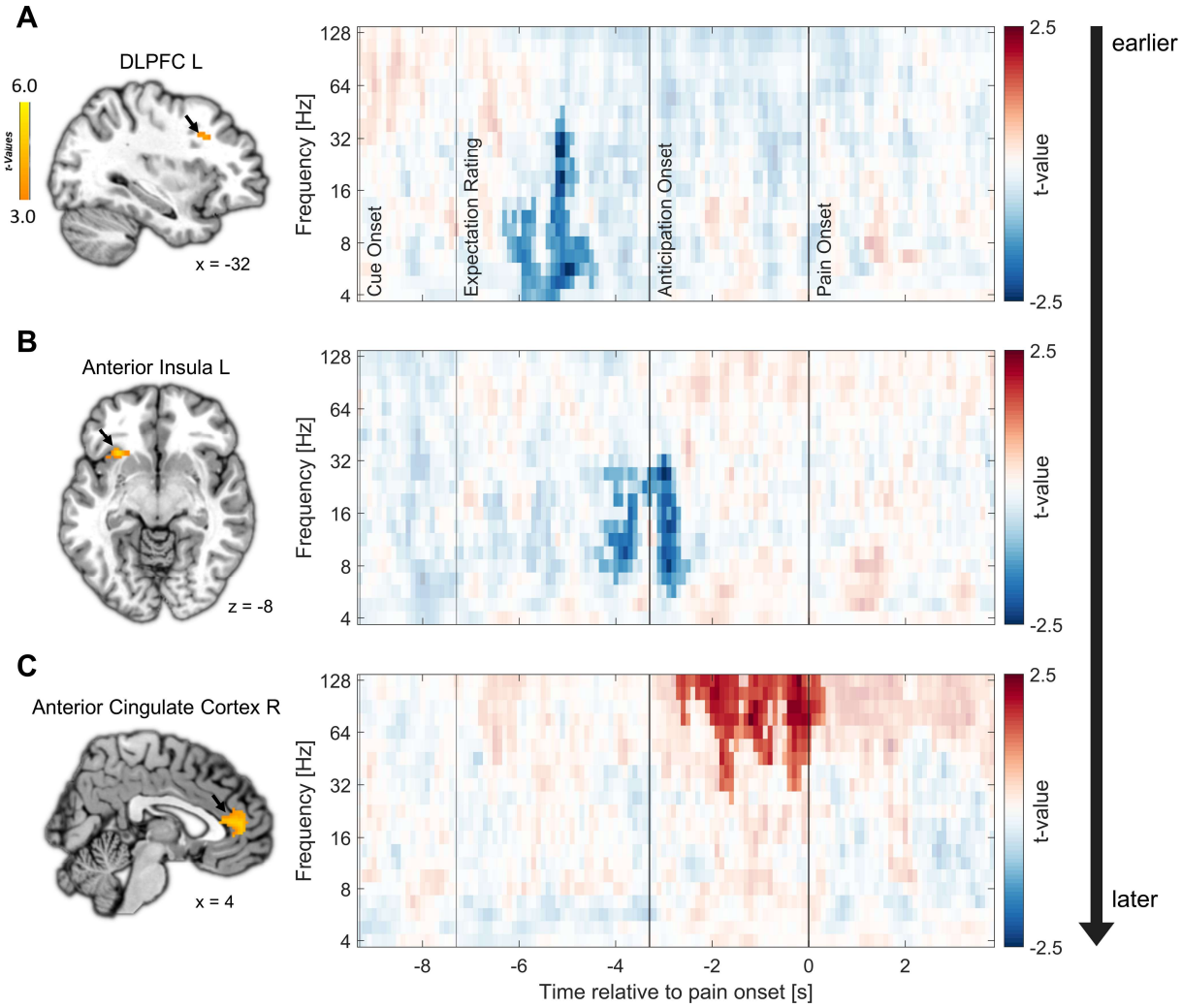

Relation of fMRI activity with EEG oscillatory power.

Correlation of single-trial hemodynamic responses with time-frequency resolved EEG activity in the left DLPFC (A), left anterior insula (B), and left ACC (C) during the anticipation phase, ordered by the timing of observed correlations as indicated by the arrow on the right. Single-trial beta weights were extracted from spherical ROIs (10 mm radius) centered around the peak voxels based on the comparison of beta weights from the FIR model between expectation and no expectation during the anticipation phase, as shown on the left ($p < .001$ uncorrected for display purposes). On the right, the cluster-corrected correlation of oscillatory power with fMRI activity averaged over all cluster electrodes is depicted. Non-significant time-frequency points are masked.

3. Discussion

The manipulation of positive, negative, or no expectations on a trial-by-trial basis allowed for a detailed analysis of their neural representations during the generation and integration of expectations with the nociceptive input. Our results revealed fundamental differences between the anticipation and pain phase, indicating the involvement of divergent processes. During the anticipation phase, valence-neutral representations were observed in areas of the DPMS and the anterior insula. After the onset of the nociceptive stimulus these areas showed differentiated representations indicating separate processes for the formation of expectations and their integration within stimulus processing. The excellent temporal resolution of our fMRI-informed EEG measures further revealed a temporal sequence of expectation processing during the anticipation phase, with an early effect within the DLPFC, followed by activation in the anterior insula, and late effects within the ACC, in line with the occurrence of different time-sensitive sub-processes of expectation generation in this phase.

Our novel within-subjects paradigm was highly effective, as expressed by 47 out of 50 subjects consistently expecting and perceiving the intensity of pain stimuli in line with the cues that induced positive, negative or no expectations. The trial-by-trial manipulation of expectations did not only affect self-reports, but also objective markers such as skin conductance responses and scores of the SIIPS (Woo et al., 2017). The SIIPS is an indicator of neural activity that tracks differences in pain perception that go beyond pain intensity and is classically affected by placebo and nocebo interventions (Botvinik-Nezer et al., 2023; Woo et al., 2017), thus serving as an excellent manipulation check for our paradigm. In line with our expectations, the SIIPS scores discriminated between positive and negative expectations only during the pain phase

392 and not during the anticipation phase. This is a first hint at substantially different
393 processes during the two phases.

394 The neural representations of expectations differ depending on the valence of
395 the expectation, i.e. if they were positive or negative and the time period. A shift from
396 common (valence-neutral) to distinct (valence-dependent) effects was evident in areas
397 classically involved in placebo analgesia during pain processing, including the bilateral
398 DLPFC, right vmPFC, left anterior insula, and thalamus. The observation of this pattern
399 in key areas of the DPMS indicates that the activation during the anticipation phase is
400 not just mere pre-activation for later pain modulation, but that preparatory processes
401 that are distinguishable from those that occur during pain perception take place. These
402 anticipatory processes may include expectation generation and maintenance, while
403 the focus shifts towards the integration of these expectations into the sensory stream
404 and the evaluation of the percept during pain processing. The observed differentiation
405 during pain is in agreement with the few studies that looked into the neuronal
406 representations of positive and negative expectations and mainly found differential
407 effects, e.g. opposite responses or differentially modulated areas during pain
408 (Benedetti et al., 2020; Crawford et al., 2021; Koyama et al., 2005; Scott et al., 2008).

409 The network of the DPMS around the DLPFC, ACC and vmPFC appears to play
410 a pivotal role in expectation processes and in the valence-dependent modulation of
411 pain perception. One important node of this network is the DLPFC. The outstanding
412 role of the DLPFC in placebo effects is well-established and supported by numerous
413 reports of increased DLPFC activity during pain anticipation (Watson et al., 2009) as
414 well as during pain processing (Zunhammer et al., 2021). This area has been
415 classically associated with top-down-regulation and expectation modulation (Geuter et
416 al., 2017), as when its neuronal excitability is experimentally manipulated, placebo

effects can be diminished or enhanced (Egorova et al., 2015; Krummenacher et al., 2010; Tu et al., 2021). The early onset of DLPFC activity implied by the EEG analysis now suggests that the DLPFC plays an important role in the initiation of both positive and negative expectation effects within the DPMS prior to the noxious stimulation (Frisaldi et al., 2015; Geuter et al., 2017; Rossettini et al., 2023; Wager & Atlas, 2015; Wager et al., 2011). The vmPFC is another important hub within the DPMS which is suggested to integrate the input from the DLPFC and to generate affective meaning in order to maintain expectations (Geuter et al., 2017). It further modulates pain perception by directly affecting brainstem systems (Koban et al., 2017), e.g. by influencing PAG activity (Geuter et al., 2017). The notion that prefrontal areas exert top-down control over other areas of the DPMS is further supported by the earlier timing of DLPFC effects compared to the ACC (Craggs et al., 2014; Watson et al., 2009). The ACC also has a direct influence on the activity of the PAG, suggesting that the ACC is another crucial area for pain modulation (Geuter et al., 2017; Livrizzi et al., 2022). The effect of the bilateral ACC at the transition from the anticipation to the pain phase could be interpreted as a preparatory mechanism for the modulation of incoming sensory information in downstream areas, consistent with its supposed role in the DPMS (Geuter et al., 2013; Geuter et al., 2017; Kong et al., 2008). Using this framework, reports of ACC activations for both positive and negative expectations during pain anticipation could be understood as a pre-activation of the ACC for pain modulation in either direction (Rossettini et al., 2023). As anticipatory activity in the ACC was related to increased gamma band power, high frequency oscillations may not only signal higher actual or perceived pain intensity during pain processing (Nickel et al., 2022; Ploner et al., 2017; Strube et al., 2021; Tu et al., 2016), but might also be important for the transfer of expectations from anticipation into pain processing.

Similarly, a shift from valence-neutral towards valence-dependent processing over time was demonstrated in the anterior insula. The insula is a key brain region involved in pain processing (e.g., Atlas & Wager, 2014; Kober et al., 2008) but is also part of several non-pain-related networks and works as multimodal network hub (Horing & Büchel, 2022). Results of the fMRI-informed EEG analysis indicated early effects in the anticipatory period consistent with an early role of the anterior insula in expectation generation and initiation. It may be speculated that the anterior insula may be responsible for integrating relevant information from different domains (e.g. from the visual cue and interoceptive information) into an expectancy signal, although it is unclear how the DLPFC and anterior insula interact in this process. Due to its connections and function within the salience network, this may involve encoding the expected threat level and salience of subsequent pain stimuli, leading to an anticipatory activation prior to the actual perceptual modulation (Taesler & Rose, 2016; Wiech et al., 2010). During pain perception, the anterior insula may then be more engaged in stimulus processing and evaluating actual salience and prediction errors in this perceptual process (Horing & Büchel, 2022), which may imply that the insula is involved in multiple tasks over time.

Similar to the anterior insula, the activation of the angular gyrus during pain processing and pain anticipation could be understood as an indicator for processes related to the formation and integration of expectations. The angular gyrus has been connected to expectation-related pain modulation only few times (e.g., Atlas & Wager, 2014; Tu et al., 2019) but its involvement is prominent in our results. Based on its presumed function in maintaining recollected multimodal representations (Jablonowski & Rose, 2022; Vilberg & Rugg, 2012), the angular gyrus may be engaged in transforming sensory information from the visual cues into expectancy signals that can be processed by e.g. the DPMS and salience network.

Based on the present results, understanding the processing of expectations requires an examination of its temporal and spatial dynamics from anticipation to pain processing, while comparing positive and negative valences to each other and to a control condition. We found largely comparable activation for positive and negative expectations during the anticipation phase, including regions outside of those classically observed in pain processing and modulation. Based on the observed temporal profiles, the DLPFC and anterior insula may be related to the top-down initiation and generation of expectations, while the ACC is activated in close proximity to pain onset as a direct link to pain modulation. During the pain phase, the focus shifts from expectation generation and maintenance towards pain modulation in either positive or negative direction, leading to distinct effects of positive and negative expectations in many areas that initially encoded expectations independently of their valence. It is not surprising that expectations are not a static process but involve different time-dependent components, as pain perception was also recently described as a complex process of interactions among multiple brain systems that are reconfigured over time (Lee et al., 2022). Expectation generation, integration and pain perception all appear to be dynamic processes, with both common and distinct routes for positive and negative expectations, depending on the time point of examination.

4. Methods

4.1. Participants

In total, 55 volunteers were recruited via an online job platform and participated in our preregistered study (German Clinical Trials Register; ID: DRKS00025872). All participants were right-handed, had normal or corrected-to-normal vision, reported no neurological or psychiatric diseases, pain conditions, current medication, substance

abuse, or pregnancy, and were non-smokers. They gave written informed consent and were compensated with 15 Euros per hour of participation. Of these 55 participants, 5 had to be excluded from all analyses (4 due to technical issues leading to the abortion of the measurement, 1 due to a severe BDI score), leading to a final sample size of *N* = 50 (*see Table 1*). As preregistered, three participants who rated expectation and pain averaged over the entire experiment higher for placebo compared to nocebo and/or stated that they did not believe in the BCI method were excluded for the analysis of neural data, as we reasoned that the analysis of expectation-related neural activity requires a successful induction of expectations. Analyses for fMRI data were performed additionally excluding 2 participants with bad MRI data (leading to *N* = 45 for fMRI analyses), and for combined EEG-fMRI analyses additionally excluding 4 participants with excessive artifacts and/or recording equipment malfunction (leading to *N* = 41 for combined EEG-fMRI analyses). The study was approved by the local ethics committee (PV7170).

Table 1

Characteristics of study participants

	Mean	SD	Range	Number (%)
Gender				
Male				18 (36%)
Female				32 (64%)
Age (years)	25.4	3.5	18 - 34	
FOP				
Severe Pain	36.5	5.4	22 - 47	
Minor Pain	18.9	4.9	10 - 33	
Medical Pain	25.8	6.4	12 - 42	
STADI				
Anxiety	15.2	4.1	10 - 28	
Depression	17.0	3.2	11 - 25	
Global Score	32.2	5.1	23 - 43	
BDI-II Global Score	6.0	3.8	0 - 16	

Note. STADI = State-Trait Anxiety Depression Inventory. FOP = Fear of Pain Questionnaire. BDI-II = Beck Depression Inventory-II.

4.2. Procedure

Pre-Measurements (Collaborative Research Centre recordings)

One day before the actual study, we recorded fMRI data (T1, functional EPI, DW EPI) and asked the participants to complete a comprehensive psychosocial questionnaire battery that will be analyzed by other projects under the structure of the overarching collaborative research center and are beyond the scope of this manuscript. Participants were pseudonymized using ALIIAS (Englert et al., 2023).

Main Experiment

The experiment consisted of four phases: a verbal instruction phase, a pain calibration phase, a conditioning phase, and a test phase. The experiment was programmed using Psychtoolbox3 (http://psychtoolbox.org/) for Matlab (Version R2021b; The MathWorks). Rating responses were given by the participants using a Button Box MR. Instructions and ratings were presented on an MR-compatible monitor with a resolution of 3840 x 2160, placed at one end of the scanner. Participants saw the monitor through a mirror that was placed approximately 12 cm away from the participant's eyes and had a distance of approximately 151 cm from the monitor. Two researchers and one radiographer guided the participants through the instructions and preparations.

Verbal Instruction Phase

After being prepared for the EEG and fMRI recording, participants were verbally informed that their current oscillatory state of the primary somatosensory cortex would be measured in real-time using a BCI (Brain Computer Interface) and that this state

would reflect their pain sensitivity. They were further told that the measured brain state would be visualized in the form of visual stimuli consisting of a brain image with the right primary somatosensory cortex highlighted in one of three different colors (green, red, or yellow). A green stimulus represented a state in which their brain would be less susceptible to pain, a red stimulus represented a state in which their brain would be highly susceptible to pain, and a yellow stimulus represented an intermediate state in which no prediction was made. With this procedure, a positive expectation was induced by the green cue, and a negative expectation was induced by the red cue. After the verbal instructions, participants were asked to fill out state questionnaires, including the State-Trait Anxiety Depression Inventory (Laux et al., 2013) and the Fear of Pain Questionnaire (McNeil & Rainwater, 1998).

Pain Calibration Phase

Heat stimuli were delivered with a PATHWAY CHEPS (Contact Heat-Evoked Potential Simulator) thermode (https://www.medoc-web.com/pathway-model-cheps), which has a rapid heating rate of 70°C/s and a cooling rate of 40°C/s and can deliver pain stimuli in the range of 30°C to 55°C in less than 300 ms. For all phases, the baseline temperature was set to 32°C, and the rise and fall rate were set to 70°C/s. The thermode head was attached to a location directly proximal to the volar mid-forearm. Using a stepwise procedure, we determined individual temperatures for each participant corresponding to values of VAS30, VAS60, and VAS70 on a visual analog scale (VAS) from 0 (“no pain”) to 100 (“unbearable pain”). Target temperatures were calculated using linear regression.

Conditioning phase

562 For the conditioning phase, the location of the thermode head was changed to
563 a location directly distal to the volar mid-forearm to avoid unnecessary sensitization of
564 one location and skin irritations. Participants were instructed that the next phase would
565 serve as the calibration of the BCI algorithm introduced in the verbal instruction phase.
566 They were informed that in this phase only green and red cues would appear because
567 the pain stimulation would only occur once a clear-cut state of their brain has been
568 detected. Each trial began with the presentation of either a red or green visual cue for
569 2 s, then the painful stimulus was administered for 4 s, and lastly, participants were
570 asked to rate their pain experience for 8 s. Between trials, there was a fully randomized
571 inter-trial interval (ITI) of between 2 and 7 s. During the painful stimulation and ITIs, a
572 fixation cross was presented in the middle of the screen. Perceived pain intensity was
573 again rated on a VAS from 0 (“no pain”) to 100 (“unbearable pain”). Unbeknownst to
574 the participants, green cues were always followed by less painful stimuli (VAS30), and
575 red cues were always followed by more painful stimuli (VAS70). They received 10
576 stimuli of each condition, leading to 20 trials in total. The order of stimuli was pseudo-
577 randomized with the restrictions of no more than two direct repetitions of the same
578 condition and the last two trials of this phase belonged to the less painful condition.
579
580 ***Test phase***
581 For the test phase, the thermode head was once again attached to the location
582 directly proximal to the volar mid-forearm. Participants were informed that the BCI
583 algorithm has now been calibrated and would be tested in the next phase. They were
584 told that the painful stimulation would occur at random predetermined points in time,
585 so that either highly pain-sensitive (red; nocebo condition), less pain-sensitive (green;
586 placebo condition), or intermediate states (yellow; control condition) could be detected
587 and reported back to the participant. The trial structure was similar to the conditioning

phase, with the change that after cue presentation, participants were asked to rate how painful they expect the next stimulus to be on a VAS ranging from 0 to 100 while the cue was still presented on the screen (4 s). After this expectation rating, a fixation cross was presented for 3.3 s (anticipation phase) before the pain stimulus was administered for 4 s (pain phase). Independently of the cue color, participants always received painful stimuli corresponding to values calibrated to VAS60. There were 30 cues of each condition followed by pain stimulation divided into three blocks, summing up to a total of 90 stimuli. Similarly to the conditioning phase, the ITI was fully randomized between 2 and 7 s. The order of cues was pseudo-randomized with no more than two direct repetitions of the same condition. Before each block, we applied one pain stimulus of VAS60 without a cue to desensitize the new skin area.

Follow-Up

One week after the main experiment, participants were invited for a follow-up measurement which is beyond the scope of this manuscript. They were asked to fill out questionnaires, including the Beck Depression Inventory-II (Beck et al., 1996; Hautzinger et al., 2006). Lastly, participants were debriefed and paid.

4.3. Data acquisition

Electrodermal Data

Electrodermal activity was measured with MRI-compatible electrodes on the thenar and hypothenar. Electrodes were connected to Lead108 carbon leads (BIOPAC Systems, Goleta, CA). The signal was amplified with an MP150 analogue amplifier (also BIOPAC Systems) and sampled at 5,000 Hz using a CED 1401 analogue-digital converter (Cambridge Electronic Design, Cambridge, UK).

614 **fMRI Data**

615 MRI was performed with a 3T Siemens PRISMA Scanner, and a 64-channel
616 head coil was used. On the day of the pre-measurements, a T1 image with the
617 following parameters was acquired: T1 FLASH 3D: TE 2.98 ms, TR: 7.1 ms, matrix flip
618 angle: 9°, FOV 25.6 * 25.6 cm, TA: 7:22 min. Two sequences on the day of the main
619 experiment were acquired: An EPI BOLD sequence and a field map sequence.
620 Participants were prepared with a 64-channel standard BrainCap MR for 3 Tesla (2020
621 Version) and the EPI BOLD sequence had therefore to be adjusted to meet the
622 necessary safety criteria. The following parameters were used: 2 D EPI BOLD: TE:
623 29.0 ms, TR: 1679.00 ms, FOV: 22.4 * 22.4 cm, flip angle: 70°, s1: 2 mm, TA: 20:17
624 min, fat saturation, 715 volumes in total; 2 D field map sequence: TR: 594 ms, TE1:
625 5.51 ms, TE2: 7.79 ms, FOV: 22.4 * 22.4 cm, flip angle: 40°, s1: 2 mm, TA: 1:31 min.

626

627 **EEG Data**

628 Continuous EEG data was recorded inside the MRI scanner using a custom 64-
629 channel BrainCap-MR for 3 Tesla using BrainVision Recorder (Version 1.10,
630 BrainProducts, Gilching, Germany). The cap contained 64 passive sintered Ag/AgCl
631 electrodes arranged according to the 10/20 System, as well as one ECG electrode.
632 FCz served as the reference and Pz served as the ground electrode. The cap was
633 connected to two Brain Amp MR plus amplifier systems with 32 channels each
634 (BrainProducts, Gilching, Germany), powered by one rechargeable battery unit.
635 Amplifiers and the battery unit were positioned on foam cushions directly behind the
636 head coil inside the scanner. Electrode skin impedance was kept below 10 kΩ. EEG
637 data was recorded with a sampling rate of 5,000 Hz and an amplitude resolution of 0.5
638 μV for EEG channels and 10 μV for the ECG channel. The EEG system was

synchronized with the clock of the MRI system using a SyncBox (BrainProducts, Gilching, Germany). The helium pump of the MRI system was switched off during data recording. Data was transmitted from the amplifiers to the recording computer outside of the scanner room via a fiber-optic cable.

4.3. Preprocessing

Electrodermal Data

Preprocessing and analysis of electrodermal data were performed using the Ledalab toolbox for MATLAB (Benedek & Kaernbach, 2010). Single-subject data was downsampled to 100 Hz and visually screened. In total, 21 subjects were excluded from the electrodermal analysis (18 due to physiological non-responsiveness, 3 due to equipment malfunction). From the remaining 26 subjects, all data segments around pain stimulation were screened for excessive artifacts, resulting in the exclusion of 55 of the 2340 segments (2.35%). Using a deconvolution method implemented in Ledalab, raw electrodermal data were decomposed into continuous phasic (driver) and tonic components. Subsequent analysis were performed on the extracted phasic skin conductance responses (SCRs). The response window for pain was determined by visual inspection of the curve to cover the peak and set between 2 and 7.5 s. SCR segments within the response window were log- and z-transformed within participants. For the log-transform, a constant (minimum of the driver plus 1) was added to the data to shift it to positive values. Lastly, segments were averaged per subject for each of the three conditions.

fMRI Data

Preprocessing of fMRI data was done using the Statistical Parameter Mapping software (SPM 12, Wellcome Department of Imaging Neuroscience, London, UK, https://www.fil.ion.ucl.ac.uk/spm/software/spm12/). The first two volumes of each block were dropped to get full MRI saturation effects. Further, realignment and unwarping, registration to standard space (Montreal Neurological Institute), and spatial smoothing with a 6 mm Gaussian kernel were used on the data.

EEG Data

MR and cardioballistic artifacts were corrected using BrainVision Analyzer 2.2 (BrainProducts, Gilching, Germany) for each block separately. Continuous MR artifacts were corrected with sliding baseline corrected average templates. Data was then downsampled to 500 Hz. Cardioballistic artifact correction was done by semi-automatically detecting a pulse template, marking it in the electrocardiogram channel, and then subtracting it from recordings.

For the remaining preprocessing and analysis, we used the Fieldtrip toolbox for Matlab (Oostenveld et al., 2011). Data were cut into trials including all relevant time intervals from 1,000 ms before cue onset to the end of pain 15,800 ms after cue onset. The resulting segmented data were low-pass filtered at 150 Hz and high-pass filtered at 0.5 Hz. We adapted a recent preprocessing approach introduced by Hipp et al. (2011). The data was split into low- and high-frequency data (34 Hz low-pass filter and 16 Hz high-pass filter, respectively) and processed in parallel. This approach leads to high sensitivity in detecting and removing artifacts from the data as e.g. heartbeats cause more artifacts at lower frequencies and muscle activity affects higher frequencies more strongly. All trials were visually inspected and removed for both subsets when containing large artifacts. Then, both high- and low-frequency data were

subjected to an independent component analysis (ICA) using a logistic infomax algorithm. Components reflecting residual cardioballistic and MR artifacts, blinks, eye- and head movement, and muscle activity were identified by visual inspection of the time course, spectrum, and topography of each component and discarded. Both subsets were re-referenced to the average of all channels and the original reference electrode was regained. Lastly, we subjected all data to another full visual scan and shifted the time axis so that the onset of pain stimulation occurred at $t = 0$ s. In total, the visual artifact screening led to the exclusion of 228 of the 3944 recorded trials (5.78%).

Time-frequency decomposition

Our procedure was again adapted from Hipp et al. (2011). Time-frequency decomposition was conducted for 21 logarithmically spaced frequencies ranging from 4 to 128 Hz (0.25-octave increments) in 0.1 s steps using the multi-taper method based on discrete prolate spheroid sequences (DPSS). The high-frequency data were used for the frequency transformation of frequencies above 25 Hz, and the low-frequency data for frequencies below 25 Hz. Temporal and spectral smoothing were adjusted to match 250 ms and 3/4 octave, respectively. This was achieved by fixing the time window to 250 ms and adjusting the number of Slepian tapers for frequencies larger than 16 Hz, while for frequencies up to 16 Hz, a single taper was used, and the time window was adjusted. We extracted single-trial time-frequency resolved data for each participant.

4.4. Data analysis

Behavioral Data

We compared differences in pain and expectation ratings for the different cue conditions by computing two repeated-measures ANOVAs with cue type (placebo vs. nocebo vs. control) as predictor and pain and expectation ratings as outcome, respectively. Partial eta-squared is used to describe effect sizes.

Electrodermal Data

We compared differences in SCRs in the pain phase by conducting a repeated-measures ANOVA with the factor cue type (placebo vs. nocebo vs. control) as predictor and SCR as outcome.

fMRI Data

Statistical inference

For each subject, a Finite Impulse Response model (FIR model) was set up on a time course of 18.4 s starting at the onset of the cue, divided into 11 bins, with a bin roughly covering the duration of one TR (1.679 s compared to 1.675 s). The FIR model was implemented separately for each condition. Data was also corrected for cardioballistic and respiratory artifacts by including them as regressors built with the RETROICOR algorithm of the PhysIO toolbox (Frässle et al., 2021; Kasper et al., 2017).

On the group level in a flexible factorial design, directed *t*-contrasts were set up for common effects (placebo and nocebo vs. control), exclusively masked with the *F*-contrast between placebo and nocebo (thresholded at $p < .05$ uncorrected) to identify areas that showed a similar response for placebo and nocebo but different to the control condition in the anticipation phase. For the comparison between placebo and nocebo, directed *t*-contrasts were set up to identify areas that showed distinct

modulation by placebo and nocebo in both anticipation and pain phase. Analyses in the anticipation phase were performed by including the FIR regressors covering the time period from -4.275 s until -0.925 s relative to pain onset (bins 4 and 5), analyses in the pain phase by including the FIR regressors covering the time from 0.75 s until 5.8 s relative to pain onset (bins 7, 8 and 9). All analyses were corrected for multiple comparisons using FWE ($p < 0.05$) correction.

ROI analyses

Additionally, ROI analyses were conducted regarding a priori hypotheses in the following areas defined by the anatomy based on the Harvard-Oxford atlas: insular cortex, thalamus, ACC, hippocampus and amygdala. Furthermore, a ROI analysis was conducted on the DLPFC based on the clusters identified in the meta-analysis conducted by Zunhammer et al. (2021) by applying a 15 mm-radius sphere around the two reported peak coordinates (xyz_{MNI}: 42, 11, 33 and xyz_{MNI}: -30, 13, 54) bilaterally.

Combined EEG-fMRI Analysis

Single-trial fMRI BOLD response amplitudes were estimated based on the pre-processed MR data using GLMsingle (Prince et al., 2022). The hemodynamic response during the anticipation phase was estimated by fitting a boxcar function with a length of 1.679 s to the anticipation onset. The accuracy of beta estimates was improved by an adaptation of GLMdenoise for single-trial beta estimation. Further, noise was reduced by using fractional ridge regression as integrated in the GLMsingle toolbox. For each trial, we extracted the mean beta within several regions of interest centered around the significant peak voxels derived from the MR analyses of common

effects of expectations during the anticipation phase. These included the left anterior insula (xyz_{MNI}: -28, 22, -6), left (xyz_{MNI}: -2, 40, -4) and right ACC (xyz_{MNI}: 4, 42, 12), right vmPFC (xyz_{MNI}: 14, 56, -14), left (xyz_{MNI}: -32, 18, 36) and right DLPFC (xyz_{MNI}: 40, 24, 36), and left thalamus (-6, -12, 4; all with 10mm sphere). For each participant on a single-trial level, Spearman's rank correlation coefficients between beta ROI estimates and time-frequency EEG data were computed, resulting in one time-frequency-resolved correlation pattern per participant and ROI. For the group level analysis, correlations were Fisher-z-transformed and tested against zero using nonparametric cluster-based permutation tests as implemented in the Fieldtrip toolbox (cluster threshold: $p = 0.05$, minimum neighbors: 2, number of randomizations: 2000). Statistics were calculated from cue onset until pain offset (-9.3 until 3.9 s relative to pain onset).

5. Data Availability

Derived data that support the findings of this study are available at https://osf.io/3g49v/. For additional information and requests, please contact the lead researcher directly.

6. Acknowledgements

This research is funded by the Deutsche Forschungsgemeinschaft (DFG, German Research Foundation): TRR 289 Treatment Expectation — Project Number 422744262, Project A03.

7. References

Adler-Neal, A. L., Emerson, N. M., Farris, S. R., Jung, Y., Coghill, R. C., & Zeidan, F. (2019). Brain moderators supporting the relationship between depressive mood and pain. *Pain*, *160*(9), 2028–2035. https://doi.org/10.1097/j.pain.0000000000001595

Amanzio, M., Benedetti, F., Porro, C. A., Palermo, S., & Cauda, F. (2013). Activation likelihood estimation meta-analysis of brain correlates of placebo analgesia in human experimental pain. *Human Brain Mapping*, *34*(3), 738–752. https://doi.org/10.1002/hbm.21471

Amanzio, M., & Palermo, S. (2019). Pain Anticipation and Nocebo-Related Responses: A Descriptive Mini-Review of Functional Neuroimaging Studies in Normal Subjects and Precious Hints on Pain Processing in the Context of Neurodegenerative Disorders. *Frontiers in Pharmacology*, *10*, 969. https://doi.org/10.3389/fphar.2019.00969

Atlas, L. Y., & Wager, T. D. (2012). How expectations shape pain. *Neuroscience Letters*, *520*(2), 140–148. https://doi.org/10.1016/j.neulet.2012.03.039

Atlas, L. Y., & Wager, T. D. (2014). A meta-analysis of brain mechanisms of placebo analgesia: Consistent findings and unanswered questions. *Handbook of Experimental Pharmacology*, *225*, 37–69. https://doi.org/10.1007/978-3-662-44519-8_3

Beck, A. T., Steer, R. A., & Brown, G. K. (1996). *Manual for the Beck Depression Inventory-II*. Psychological Corporation.

Benedek, M., & Kaernbach, C. (2010). A continuous measure of phasic electrodermal activity. *Journal of Neuroscience Methods*, *190*(1), 80–91. https://doi.org/10.1016/j.jneumeth.2010.04.028

Benedetti, F. (2014). Placebo effects: From the neurobiological paradigm to translational implications. *Neuron*, *84*(3), 623–637. https://doi.org/10.1016/j.neuron.2014.10.023

Benedetti, F., Frisaldi, E., Barbiani, D., Camerone, E., & Shaibani, A. (2020). Nocebo and the contribution of psychosocial factors to the generation of pain. *Journal of Neural Transmission (Vienna, Austria : 1996)*, *127*(4), 687–696. https://doi.org/10.1007/s00702-019-02104-x

Bingel, U., Wanigasekera, V., Wiech, K., Ni Mhuircheartaigh, R., Lee, M. C., Ploner, M., & Tracey, I. (2011). The effect of treatment expectation on drug efficacy: Imaging the analgesic benefit of the opioid remifentanil. *Science Translational Medicine*, *3*(70), 70ra14. https://doi.org/10.1126/scitranslmed.3001244

Botvinik-Nezer, R., Petre, B., Ceko, M., Lindquist, M. A., Friedman, N. P., & Wager, T. D. (2023). Placebo treatment affects brain systems related to affective and cognitive processes, but not nociceptive pain. *BioRxiv*, 2023.09.21.558825. https://doi.org/10.1101/2023.09.21.558825

Büchel, C., Geuter, S., Sprenger, C., & Eippert, F. (2014). Placebo analgesia: A predictive coding perspective. *Neuron*, *81*(6), 1223–1239. https://doi.org/10.1016/j.neuron.2014.02.042

Colloca, L., & Benedetti, F. (2007). Nocebo hyperalgesia: How anxiety is turned into pain. *Current Opinion in Anaesthesiology*, *20*(5), 435–439. https://doi.org/10.1097/ACO.0b013e3282b972fb

Colloca, L., Petrovic, P., Wager, T. D., Ingvar, M., & Benedetti, F. (2010). How the number of learning trials affects placebo and nocebo responses. *Pain*, *151*(2), 430–439. https://doi.org/10.1016/j.pain.2010.08.007

Colloca, L., Sigaudo, M., & Benedetti, F. (2008). The role of learning in nocebo and placebo effects. *Pain*, *136*(1-2), 211–218. https://doi.org/10.1016/j.pain.2008.02.006

Craggs, J. G., Price, D. D., & Robinson, M. E. (2014). Enhancing the placebo response: Functional magnetic resonance imaging evidence of memory and semantic processing in placebo analgesia. *The Journal of Pain*, *15*(4), 435–446. https://doi.org/10.1016/j.jpain.2013.12.009

Crawford, L. S., Mills, E. P., Hanson, T., Macey, P. M., Glarin, R., Macefield, V. G., Keay, K. A., & Henderson, L. A. (2021). Brainstem Mechanisms of Pain Modulation: A within-Subjects 7T fMRI Study of Placebo Analgesic and Nocebo Hyperalgesic Responses. *Journal of Neuroscience*, *41*(47), 9794–9806. https://doi.org/10.1523/JNEUROSCI.0806-21.2021

Dionisio, S., Mayoglou, L., Cho, S.-M., Prime, D., Flanigan, P. M., Lega, B., Mosher, J., Leahy, R., Gonzalez-Martinez, J., & Nair, D. (2019). Connectivity of the human insula: A cortico-cortical evoked potential (CCEP) study. *Cortex; a Journal Devoted to the Study of the Nervous System and Behavior*, *120*, 419–442. https://doi.org/10.1016/j.cortex.2019.05.019

Egorova, N., Yu, R., Kaur, N., Vangel, M., Gollub, R. L., Dougherty, D. D., Kong, J., & Camprodon, J. A. (2015). Neuromodulation of conditioned placebo/nocebo in heat pain: Anodal vs cathodal transcranial direct current stimulation to the right dorsolateral prefrontal cortex. *Pain*, *156*(7), 1342–1347. https://doi.org/10.1097/j.pain.0000000000000163

Eippert, F., Bingel, U., Schoell, E. D., Yacubian, J., Klinger, R., Lorenz, J., & Büchel, C. (2009). Activation of the opioidergic descending pain control system underlies placebo analgesia. *Neuron*, *63*(4), 533–543. https://doi.org/10.1016/j.neuron.2009.07.014

Englert, R., Schedlowski, M., Engler, H., Rief, W., Büchel, C., Bingel, U., & Spisak, T. (2023). ALIIAS: Anonymization/Pseudonymization with LimeSurvey integration and II-factor Authentication for Scientific research. *SoftwareX*, *24*, 101522. https://doi.org/10.1016/j.softx.2023.101522

Frässle, S., Aponte, E. A., Bollmann, S [Saskia], Brodersen, K. H., Do, C. T., Harrison, O. K., Harrison, S. J., Heinzle, J., Iglesias, S., Kasper, L., Lomakina, E. I., Mathys, C., Müller-Schrader, M., Pereira, I., Petzschner, F. H., Raman, S., Schöbi, D., Toussaint, B., Weber, L. A., . . . Stephan, K. E. (2021). Tapas: An Open-Source Software Package for Translational Neuromodeling and Computational Psychiatry. *Frontiers in Psychiatry*, *12*, 680811. https://doi.org/10.3389/fpsyt.2021.680811

Freeman, S., Yu, R., Egorova, N., Chen, X., Kirsch, I., Claggett, B., Kaptchuk, T. J., Gollub, R. L., & Kong, J. (2015). Distinct neural representations of placebo and nocebo effects. *NeuroImage*, *112*, 197–207. https://doi.org/10.1016/j.neuroimage.2015.03.015

Frisaldi, E., Piedimonte, A., & Benedetti, F. (2015). Placebo and nocebo effects: A complex interplay between psychological factors and neurochemical networks. *The American Journal of Clinical Hypnosis*, *57*(3), 267–284. https://doi.org/10.1080/00029157.2014.976785

Fu, J., Wu, S., Liu, C., Camilleri, J. A., Eickhoff, S. B., & Yu, R. (2021). Distinct neural networks subserve placebo analgesia and nocebo hyperalgesia. *NeuroImage*, *231*, 117833. https://doi.org/10.1016/j.neuroimage.2021.117833

Geuter, S., Eippert, F., Hindi Attar, C., & Büchel, C. (2013). Cortical and subcortical responses to high and low effective placebo treatments. *NeuroImage*, *67*, 227–236. https://doi.org/10.1016/j.neuroimage.2012.11.029

Geuter, S., Koban, L., & Wager, T. D. (2017). The Cognitive Neuroscience of Placebo Effects: Concepts, Predictions, and Physiology. *Annual Review of Neuroscience*, *40*, 167–188. https://doi.org/10.1146/annurev-neuro-072116-031132

Hautzinger, M., Keller, F., & Kühner, C. (2006). *Beck Depressions-Inventar (BDI-II). Revision.* Harcourt Test Services.

Hipp, J. F., Engel, A. K., & Siegel, M. (2011). Oscillatory synchronization in large-scale cortical networks predicts perception. *Neuron*, *69*(2), 387–396. https://doi.org/10.1016/j.neuron.2010.12.027

Horing, B., & Büchel, C. (2022). The human insula processes both modality-independent and pain-selective learning signals. *PLoS Biology*, *20*(5), e3001540. https://doi.org/10.1371/journal.pbio.3001540

Jablonowski, J., & Rose, M. (2022). The functional dissociation of posterior parietal regions during multimodal memory formation. *Human Brain Mapping*, *43*(11), 3469–3485. https://doi.org/10.1002/hbm.25861

Kasper, L., Bollmann, S [Steffen], Diaconescu, A. O., Hutton, C., Heinzle, J., Iglesias, S., Hauser, T. U., Sebold, M., Manjaly, Z.-M., Pruessmann, K. P., & Stephan, K. E. (2017). The PhysIO Toolbox for Modeling Physiological Noise in fMRI Data. *Journal of Neuroscience Methods*, *276*, 56–72. https://doi.org/10.1016/j.jneumeth.2016.10.019

Koban, L., Jepma, M., Geuter, S., & Wager, T. D. (2017). What's in a word? How instructions, suggestions, and social information change pain and emotion. *Neuroscience and Biobehavioral Reviews*, *81*(Pt A), 29–42. https://doi.org/10.1016/j.neubiorev.2017.02.014

Kober, H., Barrett, L. F., Joseph, J., Bliss-Moreau, E., Lindquist, K., & Wager, T. D. (2008). Functional grouping and cortical-subcortical interactions in emotion: A meta-analysis of neuroimaging studies. *NeuroImage*, *42*(2), 998–1031. https://doi.org/10.1016/j.neuroimage.2008.03.059

Kong, J., & Benedetti, F. (2014). Placebo and nocebo effects: An introduction to psychological and biological mechanisms. *Handbook of Experimental Pharmacology*, *225*, 3–15. https://doi.org/10.1007/978-3-662-44519-8_1

Kong, J., Gollub, R. L., Polich, G., Kirsch, I., Laviolette, P., Vangel, M., Rosen, B., & Kaptchuk, T. J. (2008). A functional magnetic resonance imaging study on the neural mechanisms of hyperalgesic nocebo effect. *Journal of Neuroscience*, *28*(49), 13354–13362. https://doi.org/10.1523/JNEUROSCI.2944-08.2008

Kong, J., Kaptchuk, T. J., Polich, G., Kirsch, I., & Gollub, R. L. (2007). Placebo analgesia: Findings from brain imaging studies and emerging hypotheses. *Reviews in the Neurosciences*, *18*(3-4), 173–190. https://doi.org/10.1515/REVNEURO.2007.18.3-4.173

Koyama, T., McHaffie, J. G., Laurienti, P. J., & Coghill, R. C. (2005). The subjective experience of pain: Where expectations become reality. *Proceedings of the National Academy of Sciences of the United States of America*, *102*(36), 12950–12955. https://doi.org/10.1073/pnas.0408576102

Krummenacher, P., Candia, V., Folkers, G., Schedlowski, M., & Schönbächler, G. (2010). Prefrontal cortex modulates placebo analgesia. *Pain*, *148*(3), 368–374. https://doi.org/10.1016/j.pain.2009.09.033

Laux, L., Hock, M., Bergner-Koether, R., Hodapp, V., & Renner, K.-H. (2013). *Das State-Trait-Angst-Depressions-Inventar: STADI; Manual.* Hogrefe.

Lee, J.-J., Lee, S., Lee, D. H., & Woo, C.-W. (2022). Functional brain reconfiguration during sustained pain. *ELife*, *11.* https://doi.org/10.7554/eLife.74463

Livrizzi, G., Lubejko, S. T., Johnson, D. A., Weiss, C. E., Patel, J., & Banghart, M. R. (2022). Prefrontal Input to the Periaqueductal Gray Controls Placebo Analgesia. *The Journal of Pain*, *23*(5), 19–20. https://doi.org/10.1016/j.jpain.2022.03.076

Lu, C., Yang, T., Zhao, H., Zhang, M., Meng, F., Fu, H., Xie, Y., & Xu, H. (2016). Insular Cortex is Critical for the Perception, Modulation, and Chronification of Pain. *Neuroscience Bulletin*, *32*(2), 191–201. https://doi.org/10.1007/s12264-016-0016-y

Manaï, M., van Middendorp, H., Veldhuijzen, D. S., Huizinga, T. W. J., & Evers, A. W. M. (2019). How to prevent, minimize, or extinguish nocebo effects in pain: A narrative review on mechanisms, predictors, and interventions. *Pain Reports*, *4*(3), e699. https://doi.org/10.1097/PR9.0000000000000699

McNeil, D. W., & Rainwater, A. J. (1998). Development of the Fear of Pain Questionnaire--III. *Journal of Behavioral Medicine*, *21*(4), 389–410. https://doi.org/10.1023/A:1018782831217

Nickel, M. M., Tiemann, L., Hohn, V. D., May, E. S., Gil Ávila, C., Eippert, F., & Ploner, M. (2022). Temporal-spectral signaling of sensory information and expectations in the cerebral processing of pain. *Proceedings of the National Academy of Sciences of the United States of America*, *119*(1). https://doi.org/10.1073/pnas.2116616119

Oostenveld, R., Fries, P., Maris, E., & Schoffelen, J.-M. (2011). Fieldtrip: Open source software for advanced analysis of MEG, EEG, and invasive electrophysiological data. *Computational Intelligence and Neuroscience*, *2011*, 156869. https://doi.org/10.1155/2011/156869

Palermo, S., Benedetti, F., Costa, T., & Amanzio, M. (2015). Pain anticipation: An activation likelihood estimation meta-analysis of brain imaging studies. *Human Brain Mapping*, *36*(5), 1648–1661. https://doi.org/10.1002/hbm.22727

Ploghaus, A., Tracey, I., Gati, J. S., Clare, S., Menon, R. S., Matthews, P. M., & Rawlins, J. N. (1999). Dissociating pain from its anticipation in the human brain. *Science (New York, N.Y.)*, *284*(5422), 1979–1981. https://doi.org/10.1126/science.284.5422.1979

Ploner, M., Sorg, C., & Gross, J. (2017). Brain Rhythms of Pain. *Trends in Cognitive Sciences*, *21*(2), 100–110. https://doi.org/10.1016/j.tics.2016.12.001

Prince, J. S., Charest, I., Kurzawski, J. W., Pyles, J. A., Tarr, M. J., & Kay, K. N. (2022). Improving the accuracy of single-trial fMRI response estimates using GLMsingle. *ELife*, *11.* https://doi.org/10.7554/eLife.77599

Rossettini, G., Campaci, F., Bialosky, J., Huysmans, E., Vase, L., & Carlino, E. (2023). The Biology of Placebo and Nocebo Effects on Experimental and Chronic Pain: State of the Art. *Journal of Clinical Medicine*, *12*(12). https://doi.org/10.3390/jcm12124113

Schmid, J., Bingel, U., Ritter, C., Benson, S., Schedlowski, M., Gramsch, C., Forsting, M., & Elsenbruch, S. (2015). Neural underpinnings of nocebo hyperalgesia in visceral pain: A fMRI study in healthy volunteers. *NeuroImage*, *120*, 114–122. https://doi.org/10.1016/j.neuroimage.2015.06.060

Scott, D. J., Stohler, C. S., Egnatuk, C. M., Wang, H., Koeppe, R. A., & Zubieta, J.-K. (2008). Placebo and nocebo effects are defined by opposite opioid and dopaminergic responses. *Archives of General Psychiatry*, *65*(2), 220–231. https://doi.org/10.1001/archgenpsychiatry.2007.34

Shi, Y., Cui, S., Zeng, Y., Huang, S., Cai, G., Yang, J., & Wu, W. (2021). Brain Network to Placebo and Nocebo Responses in Acute Experimental Lower

Back Pain: A Multivariate Granger Causality Analysis of fMRI Data. *Frontiers in Behavioral Neuroscience*, *15*, 696577. https://doi.org/10.3389/fnbeh.2021.696577

Shih, Y.-W., Tsai, H.-Y., Lin, F.-S., Lin, Y.-H., Chiang, C.-Y., Lu, Z.-L., & Tseng, M.-T. (2019). Effects of Positive and Negative Expectations on Human Pain Perception Engage Separate But Interrelated and Dependently Regulated Cerebral Mechanisms. *Journal of Neuroscience*, *39*(7), 1261–1274. https://doi.org/10.1523/JNEUROSCI.2154-18.2018

Strube, A., Rose, M., Fazeli, S., & Büchel, C. (2021). The temporal and spectral characteristics of expectations and prediction errors in pain and thermoception. *ELife*, *10.* https://doi.org/10.7554/eLife.62809

Taesler, P., & Rose, M. (2016). Prestimulus Theta Oscillations and Connectivity Modulate Pain Perception. *Journal of Neuroscience*, *36*(18), 5026–5033. https://doi.org/10.1523/JNEUROSCI.3325-15.2016

Tu, Y., Park, J., Ahlfors, S. P., Khan, S., Egorova, N., Lang, C., Cao, J., & Kong, J. (2019). A neural mechanism of direct and observational conditioning for placebo and nocebo responses. *NeuroImage*, *184*, 954–963. https://doi.org/10.1016/j.neuroimage.2018.10.020

Tu, Y., Wilson, G., Camprodon, J., Dougherty, D. D., Vangel, M., Benedetti, F., Kaptchuk, T. J., Gollub, R. L., & Kong, J. (2021). Manipulating placebo analgesia and nocebo hyperalgesia by changing brain excitability. *Proceedings of the National Academy of Sciences of the United States of America*, *118*(19), e2101273118. https://doi.org/10.1073/pnas.2101273118

Tu, Y., Zhang, L., & Kong, J. (2022). Placebo and nocebo effects: From observation to harnessing and clinical application. *Translational Psychiatry*, *12*(1), 524. https://doi.org/10.1038/s41398-022-02293-2

Tu, Y., Zhang, Z., Tan, A., Peng, W., Hung, Y. S., Moayedi, M., Iannetti, G. D., & Hu, L. (2016). Alpha and gamma oscillation amplitudes synergistically predict the perception of forthcoming nociceptive stimuli. *Human Brain Mapping*, *37*(2), 501–514. https://doi.org/10.1002/hbm.23048

Vilberg, K. L., & Rugg, M. D. (2012). The neural correlates of recollection: Transient versus sustained FMRI effects. *Journal of Neuroscience*, *32*(45), 15679–15687. https://doi.org/10.1523/JNEUROSCI.3065-12.2012

Wager, T. D., & Atlas, L. Y. (2015). The neuroscience of placebo effects: Connecting context, learning and health. *Nature Reviews Neuroscience*, *16*(7), 403–418. https://doi.org/10.1038/nrn3976

Wager, T. D., Atlas, L. Y., Leotti, L. A., & Rilling, J. K. (2011). Predicting individual differences in placebo analgesia: Contributions of brain activity during anticipation and pain experience. *Journal of Neuroscience*, *31*(2), 439–452. https://doi.org/10.1523/JNEUROSCI.3420-10.2011

Wager, T. D., Rilling, J. K., Smith, E. E., Sokolik, A., Casey, K. L., Davidson, R. J., Kosslyn, S. M., Rose, R. M., & Cohen, J. D. (2004). Placebo-induced changes in FMRI in the anticipation and experience of pain. *Science (New York, N.Y.)*, *303*(5661), 1162–1167. https://doi.org/10.1126/science.1093065

Watson, A., El-Deredy, W., Iannetti, G. D., Lloyd, D., Tracey, I., Vogt, B. A., Nadeau, V., & Jones, A. K. P. (2009). Placebo conditioning and placebo analgesia modulate a common brain network during pain anticipation and perception. *Pain*, *145*(1-2), 24–30. https://doi.org/10.1016/j.pain.2009.04.003

Wiech, K., Lin, C., Brodersen, K. H., Bingel, U., Ploner, M., & Tracey, I. (2010). Anterior insula integrates information about salience into perceptual decisions

about pain. *Journal of Neuroscience*, *30*(48), 16324–16331. https://doi.org/10.1523/JNEUROSCI.2087-10.2010

Woo, C.-W., Schmidt, L., Krishnan, A., Jepma, M., Roy, M., Lindquist, M. A., Atlas, L. Y., & Wager, T. D. (2017). Quantifying cerebral contributions to pain beyond nociception. *Nature Communications*, *8*(1), 14211. https://doi.org/10.1038/ncomms14211

Zunhammer, M., Spisák, T., Wager, T. D., & Bingel, U. (2021). Meta-analysis of neural systems underlying placebo analgesia from individual participant fMRI data. *Nature Communications*, *12*(1), 1391. https://doi.org/10.1038/s41467-021-21179-3